Fitting a Two-Component Scattering Model to Polarimetric SAR Data From Forests

Anthony Freeman, *Fellow, IEEE*

***Abstract*—Two simple scattering mechanisms are fitted to polarimetric synthetic aperture radar (SAR) observations of forests. The mechanisms are canopy scatter from a reciprocal medium with azimuthal symmetry and a ground scatter term that can represent double-bounce scatter from a pair of orthogonal surfaces with different dielectric constants or Bragg scatter from a moderately rough surface, which is seen through a layer of vertically oriented scatterers. The model is shown to represent the behavior of polarimetric backscatter from a tropical forest and two temperate forest sites by applying it to data from the National Aeronautic and Space Agency/Jet Propulsion Laboratory's Airborne SAR (AIRSAR) system. Scattering contributions from the two basic scattering mechanisms are estimated for clusters of pixels in polarimetric SAR images. The solution involves the estimation of four parameters from four separate equations. This model fit approach is justified as a simplification of more complicated scattering models, which require many inputs to solve the forward scattering problem. The model is used to develop an understanding of the ground–trunk double-bounce scattering that is present in the data, which is seen to vary considerably as a function of incidence angle. Two parameters in the model fit appear to exhibit sensitivity to vegetation canopy structure, which is worth further exploration. Results from the model fit for the ground scattering term are compared with estimates from a forward model and shown to be in good agreement. The behavior of the scattering from the ground–trunk interaction is consistent with the presence of a pseudo-Brewster angle effect for the air–trunk scattering interface. If the Brewster angle is known, it is possible to directly estimate the real part of the dielectric constant of the trunks, a key variable in forward modeling of backscatter from forests. It is also shown how, with *a priori* knowledge of the forest height, an estimate for the attenuation coefficient of the canopy can be obtained directly from the multi-incidence-angle polarimetric observations. This attenuation coefficient is another key variable in forward models and is generally related to the canopy density.**

***Index Terms*—Polarimetry, scattering mechanisms, synthetic aperture radar (SAR), tropical and temperate forests.**

I. Introduction

CLASSIFICATION, decomposition, and modeling of polarimetric synthetic aperture radar (SAR) data have received a great deal of attention in the literature [1]–[8]. The objective behind many of these efforts is to develop a better understanding of the scattering mechanisms that give rise to the polarimetric signatures seen in SAR image data.

Manuscript received August 17, 2006; revised February 28, 2007. This work was carried out by the Jet Propulsion Laboratory, California Institute of Technology, under a contract with the National Aeronautics and Space Administration.

The author is with the Jet Propulsion Laboratory, California Institute of Technology, Pasadena, CA 91109 USA.

Color versions of one or more of the figures in this paper are available online at http://ieeexplore.ieee.org.

Digital Object Identifier 10.1109/TGRS.2007.897929

In an earlier paper [9], a three-component scattering model fit to polarimetric SAR data was developed. The model was generic enough that it could be applied to any natural terrain, and it was recently evaluated in [10] to be more robust than other decompositions when applied to multiple scenes from a variety of terrains in a classification scheme. In [9], we stressed the significance of the model fit approach in understanding the multifrequency polarimetric scattering behavior observed for a tropical forest area in Belize, Central America. There has been significant progress in modeling backscatter from forested areas in recent years; nevertheless, there is still a scarcity of reliable geophysical parameters extracted from radar data. Notable success has been achieved through combining polarimetry and interferometric techniques to recover tree height (e.g., [11] and [12]). In this paper, the focus is on extracting information purely from polarimetric backscatter data. An extra dimension to the data analysis is provided through consideration of scattering behavior over a range of incidence angles—an inherent, yet often neglected, feature of the data generated by most Airborne SAR (AIRSAR) systems. The intent is to further develop our understanding of the scattering from forested areas in this type of terrain and provide a key step forward in the estimation of geophysical parameters from polarimetric radar backscatter.

Forward models (e.g., [13]–[15]) estimate radar backscatter based on modeling the forest canopy and its interactions with electromagnetic waves. These models require many inputs, as discussed in [9]. Inversion, i.e., estimating some subsets of these input parameters describing the forest from the radar backscatter data is a difficult problem, which is primarily due to the mismatch in the number of observables (the radar data) versus the number of geophysical parameters. In other words, retrieval of parameters describing the geometry of the forest canopy structure, or the dielectric properties of trunks, branches, and leaves, is a difficult problem using just polarimetric backscatter data, since there are too few measurements and too many forest parameters for a successful inversion. On the other hand, using forward models to predict backscatter values is also difficult, because the overall backscatter may not be sensitive to significant variations in forest properties. If canopy scatter dominates the return, for example, subtle changes in the double-bounce ground–trunk interaction may not be evident in the full polarization signature. A more tractable problem may be the comparison of the forward model and inversion results at the level of their contribution to the different scattering mechanisms that make up the overall backscatter, as illustrated in Fig. 1. This point of comparison problem is illustrated in the figure.

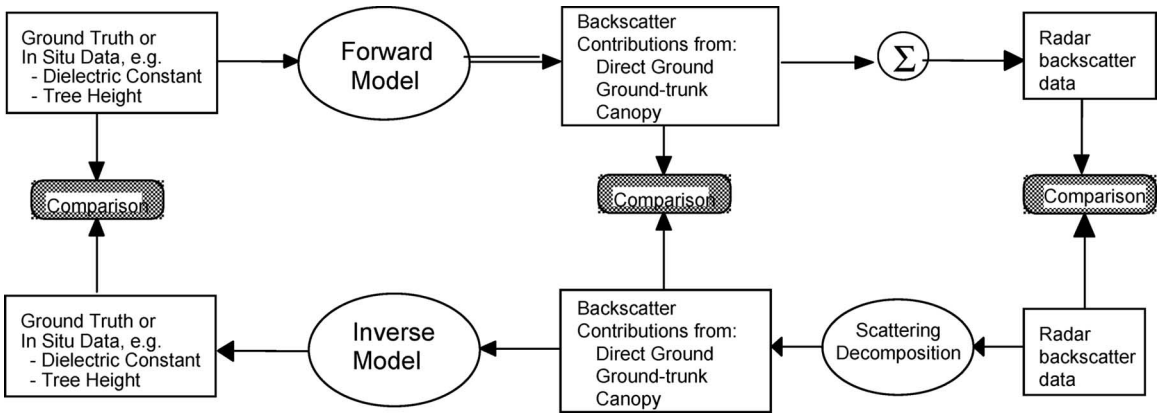

Fig. 1. Illustration of the forward and inverse scattering problem in polarimetric SAR observations of forests. Points of comparison are: at the radar image backscatter level; at the level of individual scattering mechanism contributions to the backscatter; and at the level of geophysical parameters. The point of comparison emphasized in this paper is at the scattering mechanism level, which is shown at the center of the figure.

In this paper (henceforth Freeman II), a technique for fitting a physically based two-component scattering mechanism model to ensemble averages of the polarimetric SAR data itself, without utilizing any ground truth measurements, is presented in Section II. This model is an extension of the one previously developed in [9]. The scattering mechanism components included in the model are, first, canopy scatter from, for example, randomly oriented prolate spheroids, and, then, either surface scatter directly from the ground or double-bounce scattering from a ground–trunk interaction. The two components of the scattering model are then fitted to the data, assuming that there are scenarios where either the double-bounce term or the direct ground return can be set to zero. The model fit in this paper then yields an estimate of the contribution to the total backscatter of each of the two remaining components. Based on our experience in applying the Freeman and Durden model to AIRSAR data obtained over forests, this scenario occurs often enough, especially at P-band, for an examination of a two-component model to have merit. In fact, the three-component Freeman and Durden model can be used to screen for areas in which the model described here may be most applicable.

In contrast to the Freeman and Durden model, Freeman II has an equal number of input parameters (the polarimetric radar backscatter measurements) and output parameters (the backscatter contributions from each of the two components and two parameters describing them). The model described here also has an additional degree of freedom in the canopy scattering term, which allows a broader range of canopies to be modeled, in contrast with the Freeman and Durden model, in which the canopy scattering is assumed to originate from randomly oriented dipoles. The backscatter contributions estimated from the model fit can be compared to give the relative percentage weight of each or used to estimate the contribution of each mechanism to the HH, HV, and VV backscatter terms and the HH–VV phase difference. The model can be applied to entire images or to small areas within an image to give an estimate of the relevant scattering mechanisms. Results are presented for the model fit when applied to tropical rain forest and temperate forest data obtained from the National Aeronautic and Space Agency (NASA)/Jet Propulsion Laboratory's AIRSAR in Section IV. The results from the model are shown to be in reasonable agreement with the behavior of a forward model of the ground–trunk interaction. Examining the ground–trunk interaction term in further detail, it is shown that the data are consistent with the presence of a pseudo-Brewster angle effect in the data, and an estimate for the attenuation coefficient of the canopy is derived. Finally, the paper is summarized in Section V.

II. Scattering Model

The model fit includes two (out of three) simple scattering mechanisms, as illustrated in Fig. 2. First, for canopy (or volume) scattering, it is assumed that the radar return is from a cloud of randomly oriented scatterers, exhibiting azimuthal symmetry. After [16] and [17], the covariance matrix, which is derived from the scattering matrix by forming cross-products between elements, is, for scatterers from a reciprocal medium with azimuthal symmetry (often observed in scattering from forests [18]), given by

$$\begin{pmatrix} S_{\rm hh}S_{\rm hh}^* & \sqrt{2}S_{\rm hh}S_{\rm hv}^* & S_{\rm hh}S_{\rm vv}^* \\ \sqrt{2}S_{\rm hv}S_{\rm hh}^* & 2S_{\rm hv}S_{\rm hv}^* & \sqrt{2}S_{\rm hv}S_{\rm vv}^* \\ S_{\rm vv}S_{\rm hh}^* & \sqrt{2}S_{\rm vv}S_{\rm hv}^* & S_{\rm vv}S_{\rm vv}^* \end{pmatrix} = f_c \begin{pmatrix} 1 & 0 & \rho \\ 0 & (1-\rho) & 0 \\ \rho^* & 0 & 1 \end{pmatrix}, \quad 0 \le \rho \le 1; \quad \arg(\rho) = 0\,. \quad (1)$$

In [17], (1) is shown to be applicable in the case of volume scattering from a layered random medium, particularly for randomly oriented prolate spheroidal and elliptical scatterers. Values of ρ that are higher than 1/3 tend to indicate some preferred orientation toward the vertical of the ellipsoids in the examples given in [17]. This formulation for the canopy scatter term is less restrictive than our earlier model [9], which had randomly oriented thin dipoles for the canopy scatter—a special case of (1), which was obtained by setting $\rho = 1/3$. [Note that if we take an ensemble average of the ρ parameter in (1), it is essentially the complex-valued HH–VV correlation term.]

The second scattering scattering mechanism is double-bounce scattering, e.g., from a ground–trunk interaction. As in our earlier paper, the reflection coefficients for the horizontal and vertical scatterers can be different in this model, as can the

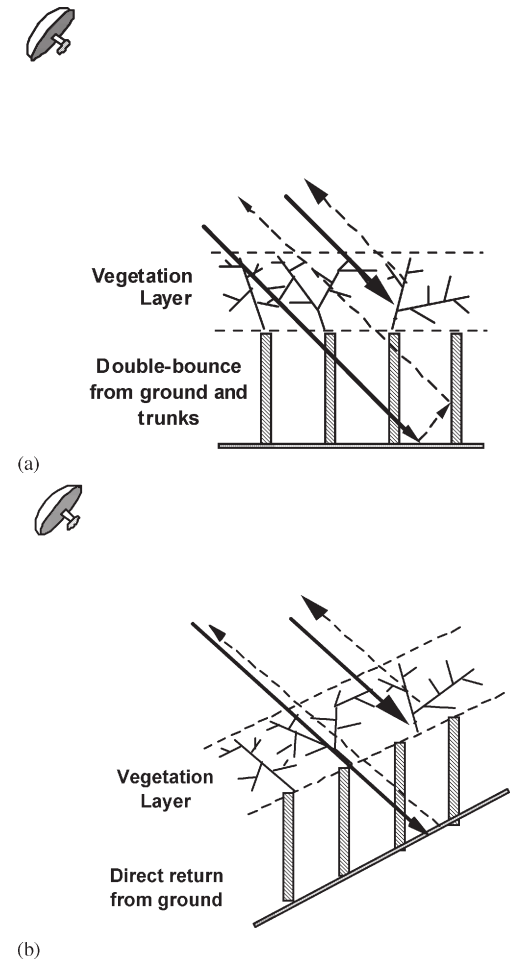

Fig. 2. Two-component scattering from a forest showing the main contributors as (a) vegetation layer scattering and double-bounce from the ground–trunk interaction or (b) vegetation layer scattering and direct ground return.

propagation delay for H and V from radar to scatter and back again. The model for double-bounce scatter is

$$\begin{pmatrix} S_{\rm hh}S_{\rm hh}^* & \sqrt{2}S_{\rm hh}S_{\rm hv}^* & S_{\rm hh}S_{\rm vv}^* \\ \sqrt{2}S_{\rm hv}S_{\rm hh}^* & 2S_{\rm hv}S_{\rm hv}^* & \sqrt{2}S_{\rm hv}S_{\rm vv}^* \\ S_{\rm vv}S_{\rm hh}^* & \sqrt{2}S_{\rm vv}S_{\rm hv}^* & S_{\rm vv}S_{\rm vv}^* \end{pmatrix} = f_g \begin{pmatrix} 1 & 0 & \alpha \\ 0 & 0 & 0 \\ \alpha^* & 0 & |\alpha|^2 \end{pmatrix}, \quad |\alpha| \le 1; \quad \arg(\alpha) \approx \pm\pi. \tag{2}$$

The third mechanism is direct surface scatter, in which the surface may be tilted in the elevation plane (but not the azimuth), for example, a sloping hillside. A phase difference between the HH and VV backscatter terms is included to model any propagation delay for H and V from radar to scatter and back again, for example, by propagation through a canopy layer or a trunk layer. The model for surface scatter is

$$\begin{pmatrix} S_{\rm hh}S_{\rm hh}^* & \sqrt{2}S_{\rm hh}S_{\rm hv}^* & S_{\rm hh}S_{\rm vv}^* \\ \sqrt{2}S_{\rm hv}S_{\rm hh}^* & 2S_{\rm hv}S_{\rm hv}^* & \sqrt{2}S_{\rm hv}S_{\rm vv}^* \\ S_{\rm vv}S_{\rm hh}^* & \sqrt{2}S_{\rm vv}S_{\rm hv}^* & S_{\rm vv}S_{\rm vv}^* \end{pmatrix} = f_g \begin{pmatrix} 1 & 0 & e^{-2j\phi}b \\ 0 & 0 & 0 \\ e^{2j\phi}b & 0 & |b|^2 \end{pmatrix}, \quad |b| \ge 1; \quad \arg(b) = 0. \tag{3}$$

Note that this has the same exact form as (2), except for the restrictions on the modulus and argument of $\boldsymbol{\alpha}$ and $\boldsymbol{b}$. This is easy to see by setting

$$\alpha = e^{-2j\phi}b. \tag{4}$$

Since (2) and (3) are mathematically equivalent, if we assume that only one is present, the model fit (when valid) should reveal which of the two mechanisms is present based on the behavior of the HH/VV amplitude and phase ratios.

Now consider the situation when only two scattering mechanisms are present, for example, canopy scatter plus double-bounce or canopy scatter plus direct surface scatter. Assuming that the two scatter components are uncorrelated and that the like- and cross-polarized returns are uncorrelated, the total second-order statistics for the two combined will be the sum of the averaged measured cross-products for each mechanism. Thus, the model for the total backscatter (where M_{pq} is the composite scattering matrix term for transmit polarization p and receive polarization q) is

$$\langle M_{\rm hh}M_{\rm hh}^*\rangle = f_c + f_g \tag{5a}$$

$$\langle M_{\rm hv}M_{\rm hv}^*\rangle = \frac{(1-\rho)}{2}f_c \tag{5b}$$

$$\langle M_{\rm vv}M_{\rm vv}^*\rangle = f_c + |\alpha|^2 f_g \tag{5c}$$

$$\langle M_{\rm hh}M_{\rm vv}^*\rangle = \rho f_c + \alpha f_g \tag{5d}$$

where f_c and f_g are the canopy and ground (double-bounce or direct) scatter contributions to the HH cross section. This model gives four equations in four unknowns (ignoring the cross-products between like- and cross-polarized terms). In general, a solution can be found, but whether that solution is consistent with the constraints on the data remains to be seen. For example, solutions that yield negative values of f_c and f_g would not be acceptable.

To solve for α, from (5a) and (5c), form

$$z_1 = \langle M_{\rm hh}M_{\rm hh}^*\rangle - \langle M_{\rm vv}M_{\rm vv}^*\rangle = f_g\left(1 - |\alpha|^2\right) \tag{6}$$

and from (5a), (5b), and (5d), we have

$$z_2 = 2\langle M_{\rm hv}M_{\rm hv}^*\rangle + \langle M_{\rm hh}M_{\rm vv}^*\rangle - \langle M_{\rm hh}M_{\rm hh}^*\rangle = (\alpha - 1)f_g. \tag{7}$$

Then to eliminate f_g, take the ratio to give

$$z_3 = \frac{z_2}{z_1} = \frac{(\alpha-1)}{(1-|\alpha|^2)} \tag{8}$$

which gives

$$\left(1 - |\alpha|^2\right)z_3 + 1 - \alpha = 0. \tag{9}$$

Taking the real and imaginary parts, we have

$$\left(1 - (x^2 + y^2)\right)\mathrm{Re}(z_3) + 1 - x = 0 \tag{10a}$$

and

$$\left(1-(x^2+y^2)\right)\mathrm{Im}(z_3)-y=0 \tag{10b}$$

where

$$x=\mathrm{Re}(\alpha)\quad y=\mathrm{Im}(\alpha).$$

After some algebraic manipulation, we have

$$x=\left(\frac{\mathrm{Re}(z_3)y}{\mathrm{Im}(z_3)}+1\right) \tag{11}$$

which, on substitution into (10b), leads to the following quadratic in y:

$$\left(\frac{\mathrm{Re}^2(z_3)}{\mathrm{Im}(z_3)}+\mathrm{Im}(z_3)\right)y^2+(2\mathrm{Re}(z_3)+1)\,y=0 \tag{12}$$

with solution

$$y=0\quad\text{or}\quad y=\frac{-\mathrm{Im}(z_3)\,(2\mathrm{Re}(z_3)+1)}{|z_3|^2}. \tag{13}$$

This solves for y the imaginary part of α. The real part of $\alpha(x)$ is derived from (11). Once α is known, f_g can be recovered using (6), and f_c from (5a). It is then straightforward to recover ρ from (5b).

Finally, the contribution of each scattering mechanism to the span P is estimated by

$$P=P_c+P_g\equiv\left(|M_{\mathrm{hh}}|^2+2|M_{\mathrm{hv}}|^2+|M_{\mathrm{vv}}|^2\right)$$

with

$$P_g=f_g\left(1+|\alpha|^2\right)$$

and

$$P_c=f_c(3-\rho). \tag{14}$$

Note that P is just four times the often used expression for total power.

The term α, as given in (2), represents the relative amplitude and phase difference between the HH and VV backscatter terms for either the direct ground return or the double-bounce case and is given by the product of a term that represents propagation through the canopy and the ratio of the HH and VV reflection terms for the direct ground return or the ground–trunk interaction. The canopy propagation term can be separated into two terms: one representing propagation through the canopy layer and the other a layer consisting only of trunks, as depicted in Fig. 2(a). The reflection terms for the direct ground or the ground–trunk term trunk can then be included so that $\boldsymbol{\alpha}$ can be written as

$$\alpha=e^{[-2(\beta_{\mathrm{h}}-\beta_{\mathrm{v}})h/\cos\theta_i]}\cdot\left[e^{j2(\gamma_{\mathrm{h}}-\gamma_{\mathrm{v}})}\right]_{\mathrm{canopy}}\cdot\left[e^{j2(\gamma_{\mathrm{h}}-\gamma_{\mathrm{v}})}\right]_{\mathrm{trunk}}\cdot(R_{\mathrm{gh}}/R_{\mathrm{gv}}) \tag{15a}$$

TABLE I
AVERAGE P-BAND BACKSCATTER VALUES AND ESTIMATED SCATTERING MECHANISM CONTRIBUTIONS FOR DIFFERENT LAND COVER TYPES FROM AIRSAR BELIZE DATA. THE F_S, F_D, AND F_V COLUMNS INDICATE THE ESTIMATED CONTRIBUTION OF EACH OF THE THREE SCATTERING MECHANISMS (SURFACE, DOUBLE-BOUNCE, AND VOLUME) IN [9]. SCATTERING SIGNATURES WHERE TWO MECHANISMS CLEARLY DOMINATE ARE SHADED BLUE IN THE CASE OF CANOPY SCATTER PLUS A DIRECT GROUND RETURN AND RED IN THE CASE OF CANOPY SCATTER PLUS A DOUBLE-BOUNCE MECHANISM

P-BAND	θ_i (deg.)	P (dB)	σ^o_{hh} (dB)	VV/HH (dB)	HV/HH (dB)	ϕ_{hhvv}* (deg.)	ρ_{hhvv}*	f_S (dB)	f_d (dB)	f_V (dB)
Open water	54.1	-24.8	-32.6	6.6	-7.4	5.8	0.33	-26.6	-35.3	-31.0
Bare soil	46.6	-18.4	-25.1	5.4	-9.5	-8.8	0.75	-19.6	-33.6	-25.4
Reeds	56.2	-16.7	-22.0	3.3	-8.6	146.7	0.27	-32.0	-25.3	-27.6
Farmland	34.9	-15.9	-20.3	2.0	-11.5	-12.5	0.53	-17.8	-23.9	-23.1
Regrowth	44.8	-10.9	-15.3	0.9	-5.8	20.7	0.25	-19.4	-21.4	-12.1
Bajo*	45.1	-9.2	-14.5	2.8	-5.8	70.8	0.21	-19.1	-15.0	-11.1
Swamp forest	47.8	-9.9	-13.8	0.6	-8.4	149.5	0.10	-17.9	-14.2	-13.2
Upland Forest	40.0	-7.7	-11.5	-0.4	-6.4	51.1	0.14	-20.7	-15.2	-8.8
Palm Forest*	36.7	-7.6	-11.3	0.1	-7.2	91.4	0.21	-24.5	-11.6	-9.8
Sedge	44.2	-6.7	-10.3	-0.5	-7.0	93.6	0.18	-18.2	-12.7	-8.3
Flooded Forest	51.9	-6.3	-9.7	-0.9	-7.0	75.6	0.16	-19.3	-13.0	-7.6
Coffee	43.1	-6.2	-9.2	-1.3	-8.8	137.3	0.40	-90.0	-9.5	-8.8
Clear-cut	46.0	-6.5	-9.0	-3.0	-8.5	31.0	0.32	-11.7	-18.0	-8.5
High Marsh Forest*	29.1	-3.8	-8.2	1.6	-7.5	-32.7	0.29	-9.0	-11.0	-6.7

or

$$\alpha=e^{[-2(\beta_{\mathrm{h}}-\beta_{\mathrm{v}})h/\cos\theta_i]}\cdot\left[e^{j2(\gamma_{\mathrm{h}}-\gamma_{\mathrm{v}})}\right]_{\mathrm{canopy}}\cdot\left[e^{j2(\gamma_{\mathrm{h}}-\gamma_{\mathrm{v}})}\right]_{\mathrm{trunk}}\cdot(R_{\mathrm{gh}}/R_{\mathrm{gv}})(R_{\mathrm{th}}/R_{\mathrm{tv}}) \tag{15b}$$

where β is an attenuation coefficient (with subscript h or v denoting polarization); the γ terms, which are real, determine the phase delay for h and v polarization as the radar pulse propagates through the canopy and the trunk layers; and h is the height of the forest. This differs from the expression given in [9], where an additional attenuation term for propagation through the canopy has been introduced, and a distinction has been drawn between the two mechanisms: direct ground return and double-bounce. After applying the model fit, this distinction can be used to determine whether the ground scattering contribution is due to direct ground return or double-bounce by investigating the behavior of the amplitude and phase of α.

III. IMPLEMENTATION

The model described in Section II can be implemented on any polarimetric SAR data set. The significance of the result will depend on how well the model describes the underlying scattering behavior. To determine where the two-component model has validity, the polarimetric scattering data were screened by applying our earlier three-component model from [9] in order to identify scatterers whose signatures were best suited for a two-component model fit. Table I, which was reproduced from [9], illustrates this approach. The results show that a two-component model would yield a good description of the scattering signatures in most cases, i.e., two scattering terms are dominant. In particular, surface scattering from a direct ground return is not an important contribution for the upland forest, palm forest, or coffee plantation.

All models have particular inconsistencies when applied to real data. Generally, the model described here was found to work best for forests for which the three-component model in

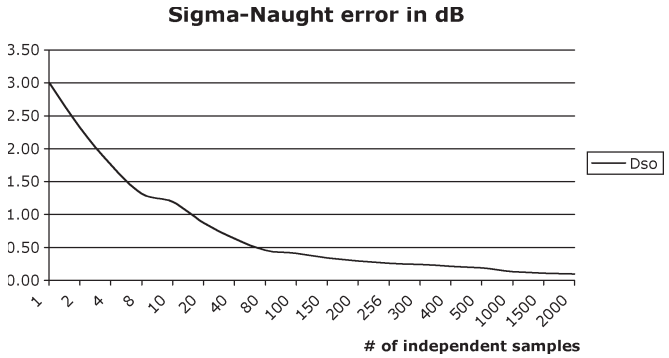

Fig. 3. Standard error in estimating sigma-naught from SAR backscatter data versus number of independent samples averaged.

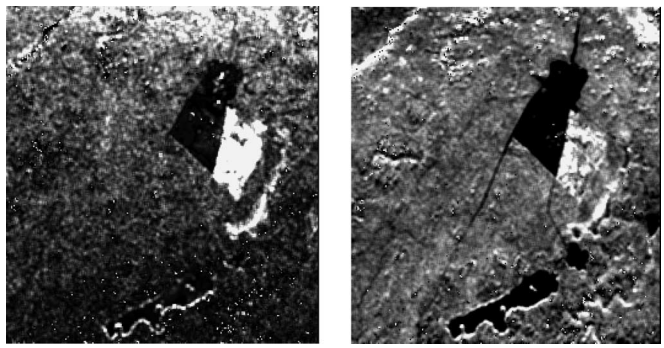

Fig. 4. Estimated contributions to the HH backscatter term from (left) ground–trunk interaction and (right) canopy from P-band data obtained over Gallon Jug, Belize.

[9] yields results that had high levels of double-bounce and canopy scatter, yet low levels of surface scatter. Some problems found in implementing the approach presented here include the following.

1) $z_1 = 0$. This occurs when the HH and VV backscatter measurements are exactly equal. This causes division by zero in estimating z_3 using (8). The solution adopted was to make z_1 a very small positive number.
2) $z_3 = 0$. This occurs when $\alpha = 1$ or the ground scattering term $f_g = 0$. This causes division by zero in estimating y using (13). The solution adopted was to make $\mathrm{Re}(z_3)$ a very small positive number, keeping $\mathrm{Im}(z_3) = 0$.
3) *Negative values for* f_c. The solution was to average over more pixels, which tended to cure the situation. For the Belize data, since the initial data were four-look, and then 4×4 averaged, a further 3×3 averaging was needed to eliminate the majority of the negative values. This is a total of 576 data values—the final product is then 120-m pixels, which is roughly 1 ha.

Averaging over many pixels was found to be essential for this process to work. The reason is primarily speckle. Consider the standard error (standard deviation) in measuring backscatter (σ^o) value from N averaged independent samples. Assuming the usual speckle distribution for one-look data (exponential distribution), this is

$$SD\left(\sigma_N^o\right) = \frac{SD(\sigma^o)}{\sqrt{N}}. \tag{16}$$

This is plotted in Fig. 3 in decibel form. With $N = 64$, the standard error is still 0.5 dB. Only after averaging 576 samples does the standard error fall below 0.2 dB. Since one of our assumptions is azimuthal symmetry, the HH and HV backscatter terms should have speckle distributions that are independent of each other. Thus, the real part of z_2, which is estimated using a difference between the HH backscatter and the HV, can have significant errors without sufficient averaging.

One of the assumptions underlying the model fit is that the like- and cross-polarized backscatter terms are uncorrelated. As noted in [19], it is often necessary to average over a large number of independent samples to recover accurate estimates of correlation coefficients in polarimetric scattering signatures. The HH–HV correlation was found to be significantly greater than zero if only 64 samples were averaged together. In fact, it only falls below 0.02 after 576 samples have been averaged.

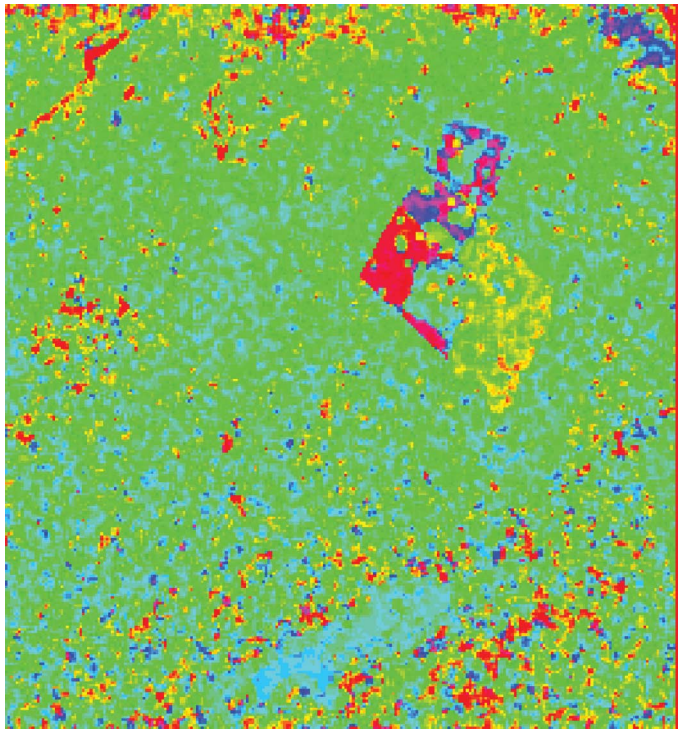

Fig. 5. HH–VV phase difference image for the ground–trunk interaction estimated from P-band data obtained over Gallon Jug, Belize. Light green phase values are $\sim 180^\circ$, bright green $\sim 140^\circ$, blue $\sim -100^\circ$, yellow $\sim 60^\circ$, and red $\sim 0^\circ$ phase difference.

IV. Data Analysis

In this section, results are presented for fitting the two-component model developed in Section II to P-band polarimetric data of tropical forest areas that were obtained over Gallon Jug, Belize, and data from two temperate forest sites.

Fig. 4 shows the separation of the contribution to the HH backscatter from the ground term and the canopy for the Gallon Jug site, whereas Fig. 5 shows the HH–VV phase difference estimated for the ground term. Note that for much of the imaged area, the HH–VV phase difference in Fig. 5 is close to $\sim 160^\circ$, indicating a ground–trunk double-bounce interaction and consistent with the HH–VV phase predicted by the forward

TABLE II
ESTIMATED SCATTERING MECHANISM CONTRIBUTIONS FOR GROUND (gd) AND CANOPY (can) AT P-BAND FOR DIFFERENT LAND COVER TYPES FROM AIRSAR BELIZE DATA

	HH (can) dB	HV(can) dB	ρ (can)	HH (gd) dB	VV (gd) dB	HH-VV Phase (gd) deg
Bare Soil	-26.7	-45.2	0.97	-32.0	-20.8	-16.8
Farmland	-20.8	-34.6	0.92	-31.6	-22.1	-139.1
Upland Forest	-12.9	-18.0	0.38	-17.2	-18.9	151.8
Swamp Forest	-15.9	-22.4	0.56	-18.1	-16.6	172.9
Coffee Plantation	-13.2	-18.1	0.35	-11.4	-13.8	149.1
Palm Forest	-13.2	-18.6	0.43	-15.9	-15.7	143.3

model in [9]. There are some notable exceptions to this: The L-shaped area to the right of the center of the image has $\sim 0^\circ$ phase, which is to be expected, since it is a bare soil field. Also, the red line cutting across the top left-hand corner of the image follows the line of sloping terrain, with a terrain slope inclined toward the top left-hand corner. This is most likely an example of a direct ground return seen beneath the forest canopy.

Table II shows the P-band model fit results using Freeman II for several different types of land cover from that paper. The results for bare soil and farmland should not be taken at the face value—results that indicate scattering contributions close to or below the noise floor for the measurement system should always be questioned, for one thing. Furthermore, in the case of farmland, the input data are ill-conditioned for the two-component model, as noted in Section III. For bare soil, the presence of a "canopy scatter" term with very low HV backscatter and a strong correlation between HH and VV (the ρ term) can best be attributed to a failure of the Small Perturbation Model to describe the scattering from that particular surface. For the forest data, the results in Table II appear consistent with the hypothesis that a two-component model can represent the polarimetric scattering behavior from a forested area over flat terrain (where the double-bounce mechanism can contribute). Note that, according to these results, the chief effect of thinning the canopy (as was done in the case of the coffee plantation at Gallon Jug) is to elevate the contribution from the double-bounce scattering mechanism by 5–6 dB—but the contribution from the canopy and the HH/VV amplitude ratio and phase difference of the double-bounce term stay the same. This suggests that the canopy contribution to the scattering is "saturated" in both cases, but that the double-bounce scattering signature is less attenuated for the thinner canopy case. Whatever the explanation, these results indicate a strong link between forest structure and the relative strengths of the canopy versus ground return.

In addition, the ρ term for the canopy scattering estimated from the four forest types takes on a range of values between 0.35 and 0.58. Referring to [17], a ρ-value close to 1/3 indicates randomly oriented scatterers in both the azimuth and vertical directions. Higher ρ-values indicate the presence of some vertical structure—for example, a statistically significant preference for vertically oriented scatterers. Hence, both the ratio of the canopy to ground return and the ρ-parameter apparently exhibit some sensitivity to forest canopy structure.

Fig. 6 shows estimates of the HH and VV backscatter measurements and HH–VV phase difference for the upland forest within the Gallon Jug image that were plotted as a function of incidence angle. These results were obtained by averaging over large rectangular homogeneous areas within the image at each incidence angle.

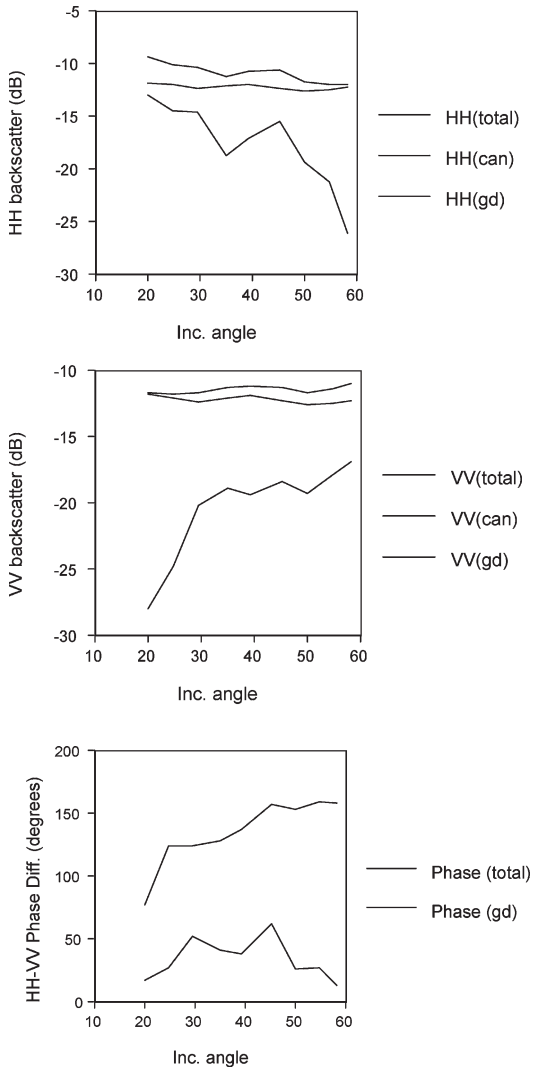

Fig. 6. Estimated contributions from ground–trunk interaction and canopy to P-band (top) HH backscatter, (middle) VV backscatter, and (bottom) HH–VV phase difference for upland forest areas as a function of incidence angle.

One feature of the data plotted in Fig. 6 is that the two-component model fit suggests that the canopy scatter term is bigger than the double-bounce term for both HH and VV polarizations at all incidence angles.

Examining the estimated HH ground term in Fig. 6, it clearly drops off as a function of incidence angle. Assuming that the HH ground backscatter term is constant over the range of θ_i (this is consistent with forward models), and with a known trunk height h, the observed falloff in the HH ground term can be modeled as $\exp(-2\beta_h h/\cos\theta_i)$, as in (15). With a canopy thickness of 25 m, the rate of falloff in Fig. 6 is then consistent with an attenuation coefficient of $\beta_{\rm h} = 0.32$ dB/m at P-band. Thus, by separating the ground term from the canopy backscatter term and using *a priori* knowledge of the forest height, an estimate for the h-polarization extinction coefficient has been derived, directly from the data itself. (For a tropical rain forest, for which the branches in the canopy have no preferred direction, we would expect that $\beta_{\rm h} = \beta_{\rm v}$.)

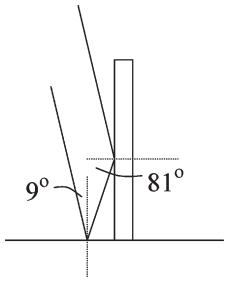

Fig. 7. Illustration of the geometry of double-bounce scattering. In the example shown, the Brewster angle occurs at an angle of 81° for the air–trunk interaction, which corresponds to an incidence angle of 9° at the air–ground interface.

There is an unusual feature in the estimated VV backscatter from the ground, which is plotted in Fig. 6. The VV ground backscatter drops off significantly with decreasing angle, from approximately -17 dB at $\theta_i \approx 58^\circ$ to -28 dB at $\theta_i \approx 20^\circ$. In addition, the estimated HH–VV phase difference also drops off from a maximum of $\sim 160^\circ$ at the larger incidence angles to $\sim 75^\circ$ for $\theta_i \approx 20^\circ$. This behavior would not be expected due to attenuation alone, so what can explain these results?

One cause could be that the double-bounce term drops off in significance compared with the canopy term at lower incidence angles. As can be seen in Fig. 6, this might explain the trend in the HH–VV phase difference. However, in Fig. 6, one would also expect to see the ratio between the HH and VV backscatter approach unity, which clearly is not the case. Another possible explanation is that the direct ground return is starting to dominate over the double-bounce. Again, the presence of a dominant direct ground return might explain the HH–VV phase difference behavior but does not fit the observed downward trend in the VV backscatter, since one would expect the VV term to increase significantly for a direct ground return for which the VV backscatter is typically greater than or equal to the HH.

Note that, for a trunk dielectric constant of $\varepsilon = 40 - 20i$, as given in [9, Table II], the Brewster angle for the trunk scattering would occur at an incidence angle of $\theta_i = \tan^{-1}(1/\varepsilon_r^{0.5}) \sim 9^\circ$ (see Fig. 7). Using the forward model for the trunk–ground interaction developed in [9] and expressed in (15), and including the estimate for the attenuation coefficient obtained earlier, one can plot the estimated behavior of the HH and VV backscatter terms from the ground–trunk term and the HH–VV phase difference, as shown in Fig. 8. The residual Brewster angle effect on both the VV backscatter and the HH–VV phase difference is clearly visible as the incidence angle tends toward zero. By comparing these results with those in Fig. 6, it can be seen that the plots from the forward model match those estimated from the data reasonably well. This implies that the trend downward in the VV ground term and the HH–VV phase difference as the incidence angle tends toward the Brewster angle is visible in the data.

Note that, by comparing Figs. 6 and 8, the closest match to the phase difference behavior extracted from the data occurs when a trunk dielectric constant of $\varepsilon = 10 - 10i$ is used in the forward model, not $\varepsilon = 40 - 20i$, as obtained from field measurements. It is worth pointing out some general properties

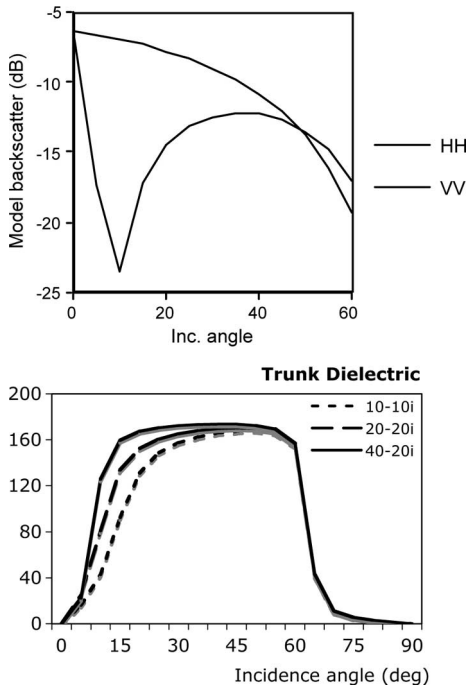

Fig. 8. Forward model predictions of HH and VV backscatter measurements and the HH–VV phase difference for the ground term at P-band for the upland forest based on the parameters from [9]. For the phase difference plots, three different values of the trunk dielectric constant are used, though the value for the ground dielectric constant is fixed at $4 - 0.5i$ in each case.

of the Fresnel reflection HH–VV phase difference for lossy dielectrics as one approaches the Brewster angle.

1) If $\varepsilon_{\rm re} \gg \varepsilon_{\rm im}$, then near the Brewster angle, the phase difference will transition sharply from $\sim 180^\circ$ to 0°.
2) As $\varepsilon_{\rm re} \rightarrow \varepsilon_{\rm im}$, then near the Brewster angle, the phase difference will transition more gradually as a function of the incidence angle from $\sim 180^\circ$ to 0°.
3) As $\varepsilon_{\rm re}$ gets smaller, then the Brewster angle also becomes smaller, and the phase transition starts at even smaller incidence angles.

Property (1) is visible in Fig. 8 for the HH–VV phase difference due to the air–soil interface, which has a sharp transition at an incidence angle of $\sim 67^\circ$. Properties (2) and (3) are most evident for the air–trunk scattering, which occurs at smaller incidence angles.

To assess whether this result was repeatable or peculiar to the Belize data set, data from another site in Raco, MI, and one in Oberpfaffenhofen, Germany, were examined, and results are plotted in Figs. 9 and 10. In each case, the VV ground scatter term exhibits a dip similar to the one shown in Fig. 8, though it is less pronounced in the Raco P-band data. The dip in the VV ground term in each plot does have a minimum at an incidence angle that is greater than what might be expected for the Brewster angle effect. For the Raco and Oberpfaffenhofen data (which have relatively sparse canopies in comparison with the Belize data), one possible explanation could be that the "true" minimum for the double-bounce term is masked by the presence of a direct ground return at smaller incidence angles. Further examination of the HH/VV amplitude ratio in each case suggests that this scenario is unlikely, since at no point does the HH/VV amplitude ratio trend toward unity (0 dB),

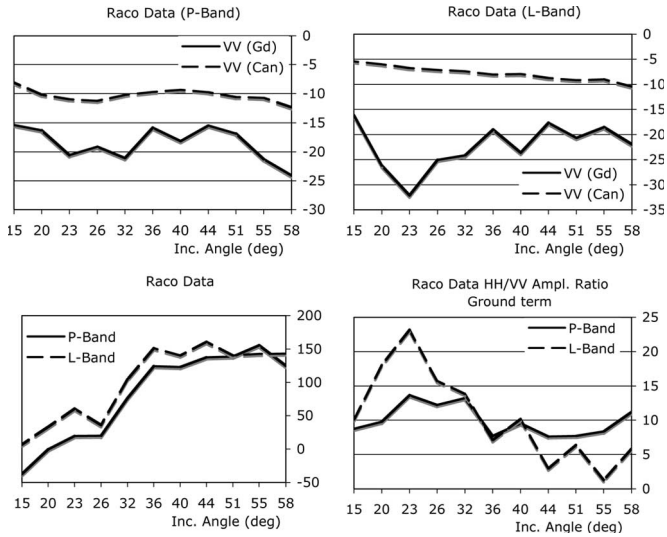

Fig. 9. P- and L-band VV ground and canopy backscatter estimates. P- and L-band HH–VV phase difference estimates and HH/VV amplitude ratios for the ground scatter term plotted as a function of incidence angle using Freeman II from AIRSAR data over forests at the Raco, MI site.

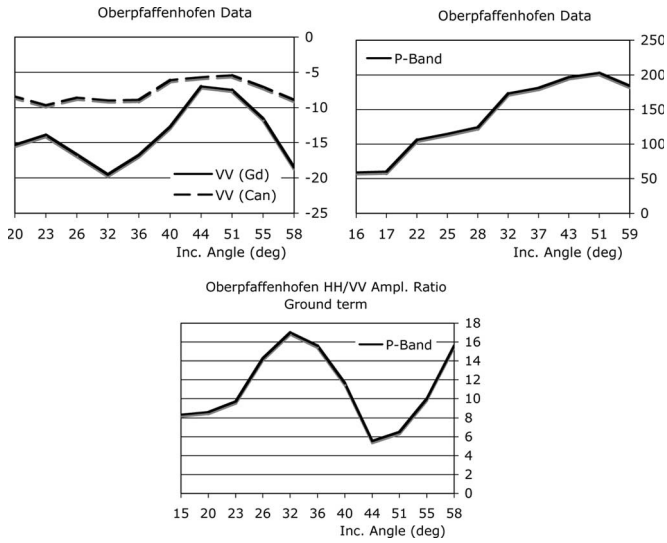

Fig. 10. P-band VV ground and canopy backscatter. HH–VV phase difference estimates and HH/VV amplitude ratios for the ground scatter term plotted as a function of incidence angle using Freeman II from AIRSAR data over forests at the Oberpfaffenhofen, Germany, site.

as would be expected for near-nadir scattering from a direct surface return [cf. (3)].

Looking at the phase difference plots in Figs. 9 and 10, the Oberpfaffenhofen data have a downward trend in the HH–VV phase difference as the incidence angle decreases (Fig. 10). The Raco site, which contains a much less dense forest, in comparison with that at Gallon Jug, was found to be suitable for estimating scattering contributions using Freeman II at both L- and P-band. The HH–VV phase at P-band in Fig. 9 can be seen to cross the zero line at an incidence angle of $\sim 20^\circ$, which, if taken as the Brewster angle, corresponds to a real part of the dielectric constant of ~ 7.5, which is not unreasonable. The behavior of the L- and P-band curves, moreover, suggests that the Brewster angle at L-band occurs at an incidence angle

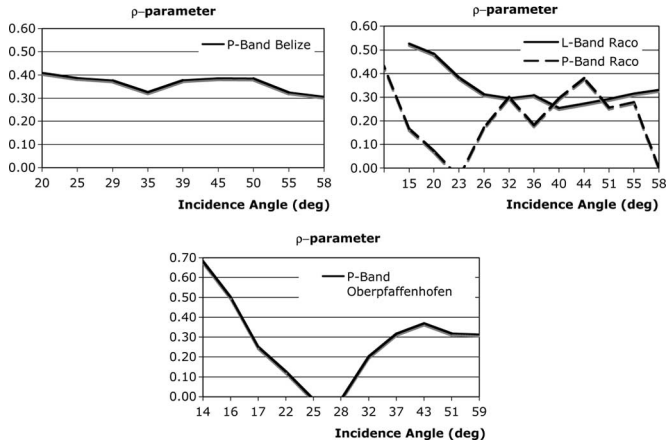

Fig. 11. ρ-parameter plotted as a function of incidence angle for the three data sets.

less than 20°, and comparison with Fig. 8 suggests that the dielectric constant at L-band is higher than at P-band.

Finally, in Fig. 11, the behavior as a function of the incidence angle of the ρ-parameter is examined. For the Belize upland forest data, ρ stays between 0.3 and 0.4 for all incidence angles, which is an indication that the original model for the canopy scatter [9], with randomly oriented dipoles, is valid. For the Raco and Oberpfaffenhofen data, the value of ρ shows a strong dependence on incident geometry. For large incidence angles, the P-band results are similar to the Belize data; but with decreasing incidence angles, ρ drops off significantly, then increases again, or increases steadily in the case of the Raco L-band data. This behavior is interesting and may represent further sensitivity to canopy structure but would need extensive ground truth and forward modeling to explain further.

V. Summary and Discussion

A new technique for fitting two simple backscatter mechanisms to polarimetric SAR data has been presented. This model-fitting approach has the advantage that it is based on the physics of radar scattering, and not a purely mathematical construct. The model does not attempt to predict the absolute level of any backscatter measurement. It matches well with the general polarimetric behavior of the scattering seen in the different forest types that are present in a P-band polarimetric data set that is obtained over a tropical rain forest site and at other sites in northern temperate forests.

The model-fitting approach worked well when fitted to the radar scattering at P-band from a tropical rain forest over a wide range of incidence angles. The approach did not work well when applied to radar scattering at L- and C-band for the same site. It is suggested that this is due to the much smaller (relative) estimated contributions from the ground or double-bounce term compared to the canopy scatter term at these shorter wavelengths, leading to estimation errors. Results for less dense forests, such as those found in temperate or boreal regions, may be more successful when applied at L-band, or even C-band. The approach put forward in the Freeman II model does not attempt to take into account the effects of surface tilt in the azimuth direction [20]—this may

have a significant impact on a direct surface return and is a topic that is worth further exploration. Another useful extension of the model would be to incorporate more sophisticated canopy models with preferred orientations built in, as in the paper by Yamaguchi *et al.* [21]. The author also looks forward to seeing results of application of the model developed here by researchers with the necessary combination of polarimetric SAR data and corresponding ground truth.

The model fit yields two parameters that appear to exhibit some sensitivity to forest canopy structure—the ratio of the canopy to ground return, which seems to be affected by canopy density, and the ρ-parameter, which, in theory, is influenced by a statistical preference for vertical orientation. This conclusion is only tentative, needing much further validation, but it is offered here because the retrieval of forest vegetation structure from remote sensing data is a "hot topic" at present, in which many researchers are engaged. It is also another point of comparison for forward models and inverse models.

For the ground–trunk backscatter term, the falloff in the VV estimate, the behavior of the HH–VV amplitude ratio, and the HH–VV phase difference were all shown to be consistent with the presence of a pseudo-Brewster angle effect for the air–trunk interaction in the data. This may be the first time that this effect has been observed in polarimetric SAR data. Forward modeling of the air–trunk interaction indicates that the "best" agreement between the two-component model fit and the forward model occurs for trunk dielectric constants where the real and imaginary parts are roughly equal, and the real part is smaller than field measurements that were obtained using a dielectric probe. This raises the following question: Is the model correct or are the field measurements? Dielectric probe measurements of tree trunks are notoriously difficult to execute—tree trunks have varying moisture levels as one probes through the bark and the xylem into the heart wood, and the dielectric constant value obtained is therefore strongly dependent on the insertion depth of the probe. The model results presented here indicate that the effective dielectric constant of the trunks is less than the value obtained by probe measurements—direct measurements in a controlled setting of the air–trunk Fresnel reflection coefficients at the appropriate wavelength would seem to be the best way to resolve this discrepancy and demonstrate the model's validity. Where the model is valid, knowledge of the Brewster angle for the air–trunk scattering term leads directly to an estimate for the real part of the dielectric constant for the trunks, as outlined in Section IV.

Using *a priori* knowledge of the forest height at the Gallon Jug site, the behavior of the estimated ground-trunk contributions to the HH backscatter as a function of incidence angle can be used to derive an estimate for the one-way attenuation coefficient of the canopy of 0.32 dB/m. This estimate is, however, significantly higher than some attenuation coefficients for forests at P-Band reported in the literature, e.g., [22]–[24], but comparable with others, e.g., [25]. Whether this is due to differences in the type of forest or to an inherent flaw in the model used here is indeterminate. It may be, for example, that the forward scattering term off the ground is dependent on the incidence angle, or the attenuation may be different for H and V polarizations. Further verification would require a repeat experiment during which attenuation coefficients are measured in the field at the same time as the P-band backscatter. If such verification were positive, this approach to estimating the attenuation coefficient could be used for other forest types, provided the forest height is known and the canopy can be considered homogeneous. For example, if such an experiment could be repeated for a flooded forest, this would constrain the ground scattering so that the attenuation through the canopy could be estimated. This is especially of interest, because forest height data can be obtained from other remote sensing techniques e.g., from radar interferometry [11], [12] or using lidar measurements [26].

Finally, the results presented in this paper should serve as a useful reminder that there is potentially valuable information contained in polarimetric backscatter measurements from diverse incidence angles, as generated by many AIRSAR systems, which generally have a wide field of view in elevation. Based on the model fit approach, it was shown how it may be possible to retrieve two physical parameters from polarimetric SAR data: the real part of the dielectric constant of the trunks and the attenuation coefficient through the canopy. An analysis of two of the model fit parameters suggests sensitivity to two different aspects of vegetation 3-D structure: canopy density and vertical orientation. These results are very tentative and require much further validation. However, in the literature relating to estimation of forest characteristics from radar data, there is much emphasis on the promise of polarimetric interferometry, and much thought has been expended on the design of repeat-pass experiments to realize that potential. Similar attention paid to the design of experiments that take advantage of incidence angle diversity in polarimetry, which was obtained on a single pass (over a homogeneous area) or multiple passes, could also yield great benefits, as suggested here.

ACKNOWLEDGMENT

The author would like to thank the anonymous reviewers for their helpful suggestions to improve the paper, C. Dobson of the NASA Headquarters for some helpful discussions on this subject, and B. Chapman for his initial suggestion that it may be possible to find the pseudo-Brewster angle effect in double-bounce scattering.

REFERENCES

[1] J. R. Huynen, "Phenomological theory of radar targets," Ph.D. dissertation, Tech. Univ., Delft, The Netherlands, 1970.

[2] J. J. van Zyl, "Unsupervised classification of scattering behavior using radar polarimetry data," *IEEE Trans. Geosci. Remote Sens.*, vol. 27, no. 1, pp. 36–45, Jan. 1989.

[3] S. R. Cloude, "Uniqueness of target decomposition theorems in radar polarimetry," in *Direct and Inverse Methods in Radar Polarimetry, Part 1*, W.-M. Boerner *et. al.*, Eds. Norwell, MA: Kluwer, 1992, pp. 267–296. NATO-ARW.

[4] W. A. Holm and R. M. Barnes, "On radar polarization mixed state decomposition theorems," in *Proc. U.S.A. Nat. Radar Conf.*, Apr. 1988, pp. 248–254.

[5] J. J. van Zyl, "Application of Cloude's target decomposition theorem to polarimetric imaging radar data," in *Proc. SPIE—Radar Polarimetry*, San Diego, CA, Jul. 1992, vol. 1748, pp. 184–212.

[6] S. R. Cloude and E. Pottier, "A review of target decomposition theorems in radar polarimetry," *IEEE Trans. Geosci. Remote Sens.*, vol. 34, no. 2, pp. 498–518, Mar. 1996.

[7] E. Krogager, "Aspects of polarimetric radar imaging," Ph.D. dissertation, Tech. Univ. Denmark, Lyngby, Denmark, May 1993. published by the Danish Defence Research Establishment.
[8] E. Krogager and Z. H. Czyz, "Properties of the sphere, diplane, helix decomposition," in *Proc. 3rd Int. Workshop Radar Polarimetry (JIPR)*, Nantes, France, Mar. 1995, pp. 106–114.
[9] A. Freeman and S. Durden, "A three-component scattering model for polarimetric SAR data," *IEEE Trans. Geosci. Remote Sens.*, vol. 36, no. 3, pp. 963–973, May 1998.
[10] J.-S. Lee, M. R. Grunes, E. Pottier, and L. Ferro-Famil, "Unsupervised terrain classification preserving polarimetric scattering characteristics," *IEEE Trans. Geosci. Remote Sens.*, vol. 42, no. 4, pp. 722–731, Apr. 2004.
[11] S. R. Cloude and K. P. Papathanassiou, "Polarimetric SAR interferometry," *IEEE Trans. Geosci. Remote Sens.*, vol. 36, no. 5, pp. 1551–1565, Sep. 1998.
[12] J. M. Kellndorfer, W. S. Walker, L. E. Pierce, M. C. Dobson, J. Fites, C. Hunsaker, J. Vona, and M. Clutter, "Vegetation height derivation from shuttle radar topography mission and national elevation data sets," *Remote Sens. Environ.*, vol. 93, no. 3, pp. 339–358, 2004.
[13] Y. Wang, "Radar backscatter modeling and applications in forested environments," Ph.D. dissertation, Univ. California, Santa Barbara, CA, Jul. 1992.
[14] F. T. Ulaby, K. Sarabandi, K. C. McDonald, M. Whitt, and M. C. Dobson, "Michigan Microwave Canopy Scattering Model (MIMICS)," *Int. J. Remote Sens.*, vol. 11, no. 7, pp. 1223–1253, 1990.
[15] F. T. Ulaby, D. Held, M. C. Dobson, K. C. McDonald, and T. B. A. Senior, "Relating polarization phase difference of SAR signals to scene properties," *IEEE Trans. Geosci. Remote Sens.*, vol. GRS-25, no. 1, pp. 83–92, Jan. 1987.
[16] S. H. Yueh, R. Kwok, and S. V. Nghiem, "Polarimetric scattering and emission properties of targets with reflection symmetry," *Radio Sci.*, vol. 29, no. 6, pp. 1409–1420, 1994.
[17] S. V. Nghiem, S. H. Yueh, R. Kwok, and F. K. Li, "Symmetry properties in polarimetric remote sensing," *Radio Sci.*, vol. 27, no. 5, pp. 693–711, Sep./Oct. 1992.
[18] J.-C. Souyris, P. Imbo, R. Fjørtoft, S. Mingot, and J.-S. Lee, "Compact polarimetry based on symmetry properties of geophysical media: The $\pi/4$ mode," *IEEE Trans. Geosci. Remote Sens.*, vol. 43, no. 3, pp. 634–646, Mar. 2005.
[19] R. Touzi, A. Lopes, J. Bruniquel, and P. W. Vachon, "Coherence estimation for SAR imagery," *IEEE Trans. Geosci. Remote Sens.*, vol. 37, pt. 1, no. 1, pp. 135–149, Jan. 1999.
[20] J. S. Lee, D. Schuler, T. L. Ainsworth, E. Krogager, D. Kasilingam, and W. M. Boerner, "On the estimation of radar polarization orientation shifts induced by terrain slopes," *IEEE Trans. Geosci. Remote Sens.*, vol. 40, no. 1, pp. 30–41, Jan. 2002.
[21] Y. Yamaguchi, T. Moriyama, M. Ishido, and H. Yamada, "Four-component scattering model for polarimetric SAR image decomposition," *IEEE Trans. Geosci. Remote Sens.*, vol. 43, no. 8, pp. 1699–1706, Aug. 2005.
[22] J. G. Fleischman, S. Ayasli, E. M. Adams, and D. R. Gosselin, "Foliage penetration experiment: Part I—Foliage attenuation and backscatter analysis of SAR imagery," *IEEE Trans. Aerosp. Electron. Syst.*, vol. 32, no. 1, pp. 135–144, Jan. 1996.
[23] B. T. Binder, M. F. Toups, S. Ayasli, and E. M. Adams, "SAR foliage penetration phenomenology of tropical rain forest and northern U.S. forest," in *Proc. IEEE Radar Conf.*, 1995, pp. 158–163.
[24] B. Ferrell, "Ultrawideband foliage penetration measurements," in *Proc. IEEE Radar Conf.*, 1994, pp. 80–84.
[25] P. Dubois-Fernandez *et al.*, "The specificity of P Band PolInSAR data over vegetation," in *Proc. of PolINSAR Workshop*, Frascati, Italy, Jan. 2007.
[26] B. Koetz, F. Morsdorf, G. Sun, K. J. Ranson, K. Itten, and B. Allgowerf, "Inversion of a lidar waveform model for forest biophysical parameter estimation," *IEEE Geosci. Remote Sens. Lett.*, vol. 3, no. 1, pp. 49–53, Jan. 2006.

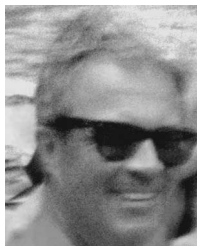

Anthony Freeman (M'83–SM'94–F'00) received the B.Sc. (Hons.) degree in mathematics and the Ph.D. degree in astrophysics from the University of Manchester, Manchester, U.K., in 1979 and 1982, respectively.

He is currently the Earth Science Research and Advanced Concepts Program Manager at the Jet Propulsion Laboratory (JPL), California Institute of Technology, Pasadena. JPL has a broad portfolio of Earth Science missions, as well as planetary science missions, and this office is responsible for all of JPL's future work in this area. Prior to this position, he was the Section Manager of the Mission and Systems Architecture Section at JPL, where he was responsible for all advanced mission studies at JPL, and prior to this, he was the Instrument Manager for the LightSAR Radar Program at JPL. His research interests include correction of Faraday rotation, modeling of polarimetric radar scattering signatures, and the design of P-band spaceborne SARs. He is the holder of two patents.

Dr. Freeman received the NASA Exceptional Service Medal for calibration of SIR-C mission data and has received numerous NASA new technology awards.